

# Comparison of Integrated Water Vapor from GNSS and radiosounding at four GRUAN stations

Javier Vaquero-Martínez<sup>1</sup>, Manuel Antón

*Departamento de Física, Universidad de Extremadura, Badajoz (Spain)*

*Instituto Universitario de Investigación del Agua, Cambio Climático y Sostenibilidad (IACYS), Universidad de Extremadura, Badajoz (Spain)*

José Pablo Ortiz de Galisteo

*Agencia Estatal de Meteorología (AEMET), Valladolid (Spain)*

*Grupo de Óptica Atmosférica, Universidad de Valladolid, Valladolid (Spain)*

Roberto Román, Victoria E. Cachorro, David Mateos

*Grupo de Óptica Atmosférica, Universidad de Valladolid, Valladolid (Spain)*

---

## Abstract

Integrated water vapor (IWV) data from Global Navigation Satellite Systems (GNSS) and radiosounding (RS) are compared over four sites (Lindenberg, Ny-Alesund, Lauder and Sodankyla), which are part of the Global Climate Observing System (GCOS) Reference Upper Air Network (GRUAN). Both datasets show an excellent agreement, with a high degree of correlation ( $R^2$  over 0.98). Dependences of GNSS-RS differences on several variables are studied in detail. Mean bias error (MBE) and standard deviation (SD) increase with IWV, but in relative term, these variables decrease as IWV increases. The dependence on solar zenith angle (SZA) is partially related to the distribution of IWV with SZA, but the increase of SD for low SZA could be associated with errors in the humidity sensor. Large surface pressures worsen performance, which could be due to the fact that low IWV is typically present in high pressure situations. Cloud cover shows a weak influence on the mentioned MBE and SD.

---

<sup>1</sup>javier\_vm@unex.es

The horizontal displacement of radiosondes generally causes SD to increase and MBE to decrease (increase without sign), as it could be expected. The results point out that GNSS measurements are useful to analyze performance to other instruments measuring IWV.

---

## 1. Introduction

Water vapor has a paramount relevance in the climate system, since it is acknowledged as the most important atmospheric greenhouse gas, and despite of not being directly involved in global warming, it causes a positive radiative feedback on climate system (Colman, 2003, 2015). It also plays a fundamental role in energy transport, evaporating at low latitudes, and being transported to higher latitudes where it condensates, releasing high amounts of latent heat (Myhre et al., 2013).

Integrated water vapor (IWV) is the variable commonly used to study the atmospheric water vapor. IWV is a magnitude equivalent to condensing all the water vapor in the atmospheric vertical column and measuring the height that it would reach if contained in a vessel of unit cross section; being its units those of superficial density ( $\text{g mm}^{-2}$ ) or length (mm).

However, understanding of water vapor effects on climate still needs improving because of the high variability of this gas, both spatially and temporally. It is therefore necessary to retrieve quality water vapor data. Radiosounding (RS) is one of the more precise and direct ways to measure water vapor profiles, and from them IWV data, despite its limitation of temporal resolution (typically one or two launches per day). RS is therefore established as a reference to validate other instruments (du Piesanie et al., 2013; Ohtani & Naito, 2000; Ant3n et al., 2015). However, it still has some sources of errors as explained in Wang & Zhang (2008) and Dirksen et al. (2014), most of them due to the problem of changes in the radiosonde models and errors in the humidity sensor related to heating by solar radiation.

Moreover, Global Navigation Satellite Systems (GNSS) meteorology is a

26 relatively recent technique that can be used to derive IWV data (Bevis et al.,  
27 1992). GNSS measurements have some advantages: all-weather availability,  
28 high temporal resolution (5 min to 2 hourly), high accuracy (less than 3 mm in  
29 IWV) and long-term stability. Hence, GNSS data are also used as reference to  
30 validate other instruments (Köpken, 2001; Prasad & Singh, 2009; Rama Varma  
31 Raja et al., 2008; Román et al., 2015; Vaquero-Martínez et al., 2017a,b, 2018),  
32 but as the recent technique that it is, GNSS meteorology still needs validation  
33 and assessment of quality in different parts of the Globe.

34 The Global Climate Observing System (GCOS) Reference Upper-Air Net-  
35 work (GRUAN) has recognized the need of having redundant water vapor mea-  
36 surements in order to improve their quality (GRUAN, 2007). Hence, GRUAN  
37 stations that already measure water vapor with RS are being equipped with  
38 GNSS receivers and a GRUAN GNSS water vapor product is being developed  
39 (WMO, 2008).

40 The main goal of this study is to analyze the possible errors of the new  
41 GNSS IWV products in order to assess their use for other purposes, allowing an  
42 improvement in temporal resolution as compared with traditional RS. This way,  
43 in this article compare the IWV from GNSS against IWV from RS at the four  
44 GRUAN stations with both RS and GNSS water vapor data currently available,  
45 and analyze the causes of the differences.

46 This article is organized as follows: Section 2 describes the different datasets  
47 used and their characteristics, and the methodology used in this work. Section 3  
48 includes the results and its discussion, validating the GNSS retrieval performed  
49 by the authors for comparison purposes, and analyzing the comparison results.  
50 Section 4 summarizes the main conclusions.

## 51 **2. Material and methods**

### 52 *2.1. IWV from GRUAN GNSS*

53 GNSS consists of a series of satellites that communicate through L-band  
54 microwave radiation with receivers, mainly in order to estimate these receivers'

55 locations. The method to obtain IWV from GNSS measurements is detailed in  
56 Bevis et al. (1992), and briefly explained in the following lines.

57 The time spent by the signal in reaching the receiver can be used to calculate  
58 the distance between the satellite and receiver, and taking into account the  
59 position of the satellites, to obtain the receiver's position. However, several  
60 corrections need to be applied, since the signal suffers a series of delays in its  
61 travel to the receiver. There is a particular contribution, the Slant Tropospheric  
62 Delay (STD), that allows IWV calculation. This contribution refers to the delay  
63 that the troposphere causes in the signal, and is referred to the path that the  
64 signal follows. Mapping functions (Niell, 2000; Boehm et al., 2006a,b) can be  
65 applied to obtain the zenithal equivalent of this amount, the Zenith Tropospheric  
66 Delay (ZTD). ZTD is the sum of two contributions, one related to the non-  
67 dipolar contribution of all gases in the troposphere (Zenith Hydrostatic Delay,  
68 ZHD), and another related to the dipolar contribution of water vapor (Zenith  
69 Wet Delay, ZWD) since it is the only compound with dipolar momentum in  
70 the atmosphere. A simple model can estimate accurately ZHD (Saastamoinen,  
71 1972), based on surface pressure. This model is accurate to the submillimeter  
72 region except if that the hydrostatic equilibrium condition does not hold; in  
73 that case errors can reach 1 mm in ZHD. The performance of other models are  
74 similar (Opaluwa et al., 2013). Once ZHD is obtained, ZWD can be estimated  
75 as  $ZWD = ZTD - ZHD$ .

76 Additionally, another variable is necessary to convert ZWD to IWV, the  
77 water vapor weighted mean temperature in the vertical column ( $T_m$ ).  $T_m$  is  
78 defined as Eq. (1):

$$T_m = \frac{\int \frac{P_v}{T} dz}{\int \frac{P_v}{T^2} dz}, \quad (1)$$

79 where  $P_v$  is water vapor partial pressure and  $T$  is the temperature, both at  
80 altitude  $z$ .  $T_m$  is often estimated from surface temperature from meteorological  
81 stations, using empirical fits, or obtained from re-analysis or radiosondes.

82 The product used in this work is developed by GRUAN GNSS (GG) Precip-

83 itable Water Vapour Task Team. Ground-based GNSS IWV has been identified  
84 as a Priority 1 measurement for GRUAN. Therefore, a lot of efforts are being  
85 done in the last few years to implement this kind of measurements in GRUAN  
86 sites. The sites are Lindenberg (LIN), Sodankylä (SOD), Lauder (LAU) and  
87 Ny-Ålesund (NYA). Despite the voluntary nature of GG sites, the GG sites  
88 must follow a series of guidelines in order to ensure the quality of GG IWV  
89 data. Thus, these sites must be equipped with automatic meteorological sta-  
90 tions or there must be a nearby station. The GG locations involved in this work  
91 are detailed in Table 1.

92 GRUAN network provides both ZTD and IWV products for those stations  
93 equipped with GNSS. However, sometimes meteorological data (pressure and  
94 temperature) are not available and GRUAN provides only ZTD product. The  
95 number of days with GG IWV data at every station available for this study is  
96 also shown in Table 1. It can be observed that LAU and SOD stations exhibit  
97 a reduced number of days with original GG IWV data. To solve this issue and  
98 increase the data number, in this work, GRUAN radiosonde meteorological data  
99 ( $T_m$  and surface pressure) are used to obtain a new IWV product from GG ZTD  
100 data (obtained by authors for comparison purposes only). This new product,  
101 developed for comparison purposes, is named in this work as “Re-calculated GG  
102 IWV product”, while the GNSS IWV product retrieved directly from GRUAN  
103 have been named as “Original GG IWV product”. Table 1 shows the number of  
104 available days with this re-calculated GG IWV product. It must be noted the  
105 notable increase of available days, particularly for LAU and SOD sites. Some  
106 restrictions have been applied to ensure data quality:

- 107 • Resulting values of IWV must make sense ( $0 \text{ mm} < \text{IWV} < 100 \text{ mm}$ ).
- 108 • Mean weighted temperature must be lower than 500 K and positive.

## 109 2.2. Radiosoundings from GRUAN network.

110 GRUAN network provides radiosonde data for 28 sites. We have considered  
111 those sites that also have a nearby GNSS product from GRUAN. Table 2 shows

Table 1: Location of the GNSS stations and days with IWV and ZTD data available.

Site	Corresponding RS site	Latitude ( $^{\circ}$ N)	Longitude ( $^{\circ}$ E)	Altitude (m)	Days with IWV data	Days with ZTD data
ldb0	LIN	52.124	14.070	0.002	2143	2164
ldb2	LIN	52.123	14.072	0.160	138	148
ldrz	LAU	-45.022	169.410	0.380	41	98
nya1	NYA	78.555	11.515	0.084	1873	1898
nya2	NYA	78.555	11.513	0.082	0	27
nyal	NYA	78.555	11.521	0.082	0	0
soda	SOD	67.251	26.232	0.300	36	1402
sodf	SOD	67.216	26.375	0.213	0	1

Table 2: Location of RS stations, distance to GNSS sites, and coincident period for both instruments.

Site	Latitude ( $^{\circ}$ N)	Longitude ( $^{\circ}$ E)	Altitude (m)	Distance (km)	Coincident period
LIN	52.210	14.120	112	10.2	12/11/2012 to 04/15/2015
LAU	-45.050	169.680	370	21.5	06/08/2005 to 01/22/2018
SOD	67.370	26.630	179	21.6	05/21/2006 to 05/02/2017
NYA	78.923	11.923	16	42.1	05/15/2007 to 01/10/2018

112 the locations of the four sites considered in this work.

113 Typically the radiosonde launches are at specific hours. LIN typically has 4  
 114 launches a day (00, 06, 12, 18 h), while NYA’s sondes are typically launched at  
 115 12h, and some launches at other hours, specially at 00, 06, and 18 h. Sondes at  
 116 SOD are launched at 00 and 12 h (some others at different hours), and at LAU  
 117 at different hours (approximately one launch per week).

118 The radiosondes that provide the data in this work are Vaisala RS92. The  
 119 RS92 model is equipped with a wire-like capacitive temperature sensor (“ther-  
 120 mocap”); two polymer capacitive moisture sensor (“humicap”), a silicon-based  
 121 pressure sensor and a GPS receiver. More detailed information about the  
 122 processing of the data retrieved can be found at [https://www.gruan.org/  
 123 instruments/radiosondes/sonde-models/vaisala-rs92/](https://www.gruan.org/instruments/radiosondes/sonde-models/vaisala-rs92/) or Dirksen et al.  
 124 (2014). The main error sources that affect the humidity sensor are: daytime  
 125 solar heating of the Humicaps (introduces a dry bias), sensor time-lag at temper-  
 126 atures below about  $-40^{\circ}$  (this is not a problem in this work) and temperature

127 dependent calibration correction.

128 The GRUAN RS92 product includes data on profiles of pressure, tempera-  
129 ture, humidity, relative humidity, water vapor mixing ratio, wind information,  
130 frostpoint, short-wave radiation, and associated uncertainties. IWV can be cal-  
131 culated by integration of water vapor mixing ratio (WVMR) in pressures as Eq.  
132 (2)

$$\text{IWV} = \int_0^{p_s} \text{WVMR} \cdot dp, \quad (2)$$

133 where WVMR is the water vapor mixing ratio,  $p$  is the pressure and  $p_s$  the  
134 surface pressure. In addition, some restrictions have been considered in order  
135 to ensure GRUAN data quality:

- 136 • Number of levels must be more than 15.
- 137 • First level must be at height lower than 1 km.
- 138 • Last level must be at height larger than 9 km.
- 139 • Resulting values of IWV must make sense  $0 \text{ mm} < \text{IWV} < 100 \text{ mm}$ .

### 140 *2.3. Methodology*

141 The followed criterion to match the GNSS and RS data require that time  
142 differences between RS launch and GNSS measurement must be below 30 min-  
143 utes. For the analysis of differences, RS measurements have been considered  
144 as reference and two variables have been analyzed, physical difference (GNSS  
145 minus RS) and relative difference (difference divided by RS value). The mean  
146 of the differences (also known as mean bias error, MBE) and the standard de-  
147 viation of the differences (SD) have been calculated. The SD have been used  
148 as a measurement of precision and the MBE as measurement of accuracy. The  
149 MBE is calculated as Eq. (3)

$$\text{MBE} = \frac{1}{N} \sum_i^N \delta_i, \quad (3)$$

150 where  $\delta_i$  are the physical differences (absolute MBE) or the relative differ-  
 151 ences (relative MBE). Moreover the SD is obtained as Eq. (4)

$$SD = \sqrt{\frac{1}{N-1} \sum_i^N (\delta_i - \bar{\delta}_i)^2}. \quad (4)$$

152 In order to study whether these differences depend on other variables or  
 153 not, the data have been divided into several bins of similar values of these  
 154 variables for the study of the precision and accuracy of IWV in each bin. It  
 155 must be noticed that data bins with less than 15 data have been rejected, as  
 156 not representative.

### 157 3. Results and discussion

#### 158 3.1. Original GG IWV data vs Re-calculated GG IWV data

159 Figure 1 shows the correlation between the original and re-calculated GG  
 160 IWV data. In all stations both data-sets exhibit an excellent agreement ( $R^2 \sim$   
 161 0.99). All stations show negative offsets (except NYA, which is positive), but  
 162 all are quite small, less than 0.4 mm in all cases. Outliers, like the ones in NYA  
 163 and LIN (differences of more than 1.5 mm in IWV), are mainly caused by the  
 164 differences in pressure measurements. However, around 90% of the data pairs  
 165 differ by less than 0.7 mm.

166 Therefore, the data-set of GNSS-derived IWV using meteorological data  
 167 from radiosonde (GNSSRS) represents very well GRUAN's IWV product. In  
 168 order to have a data-set with the same features, all the data used in this work will  
 169 come from the GNSS-derived IWV using meteorological data from radiosonde.  
 170 The advantages of using this data-set are:

- 171 1. More data is available (particularly at SOD and LAU stations).
- 172 2. Davis "Mean" temperature can be obtained directly from radiosonde.
- 173 3. Temporal interpolation is not necessary.



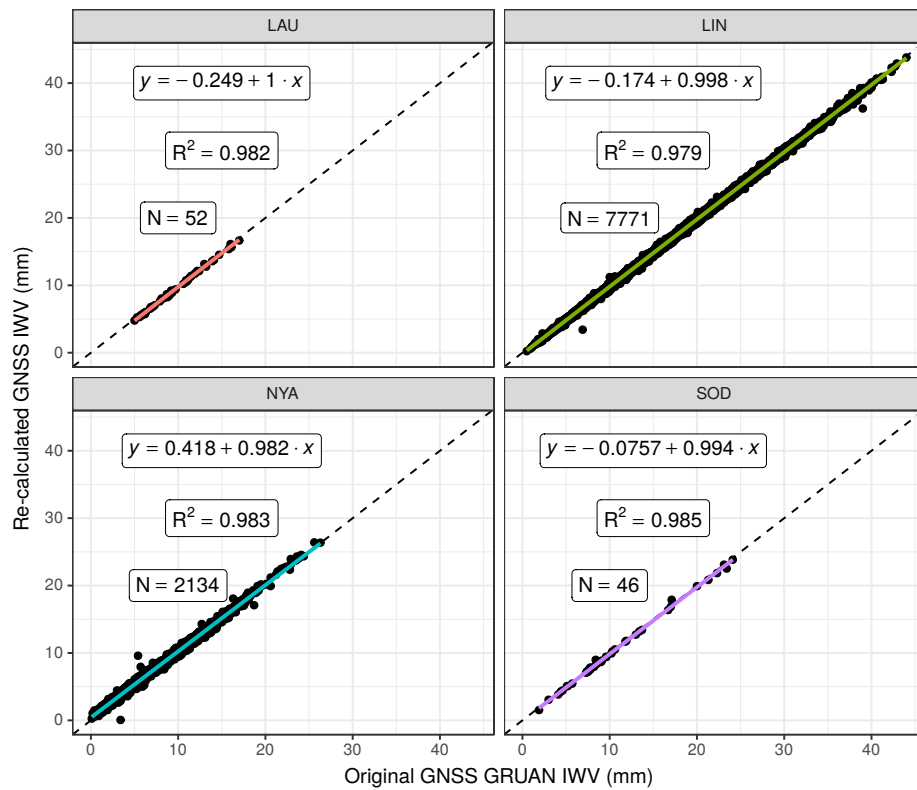


Figure 1: Scatterplots for GNSS-derived IWV from meteorological data provided by GRUAN (x-axis) and meteorological data provided by radiosounding (y-axis) for the four GRUAN stations. Color, continuous lines are regression lines and black, dashed lines are the identity line.

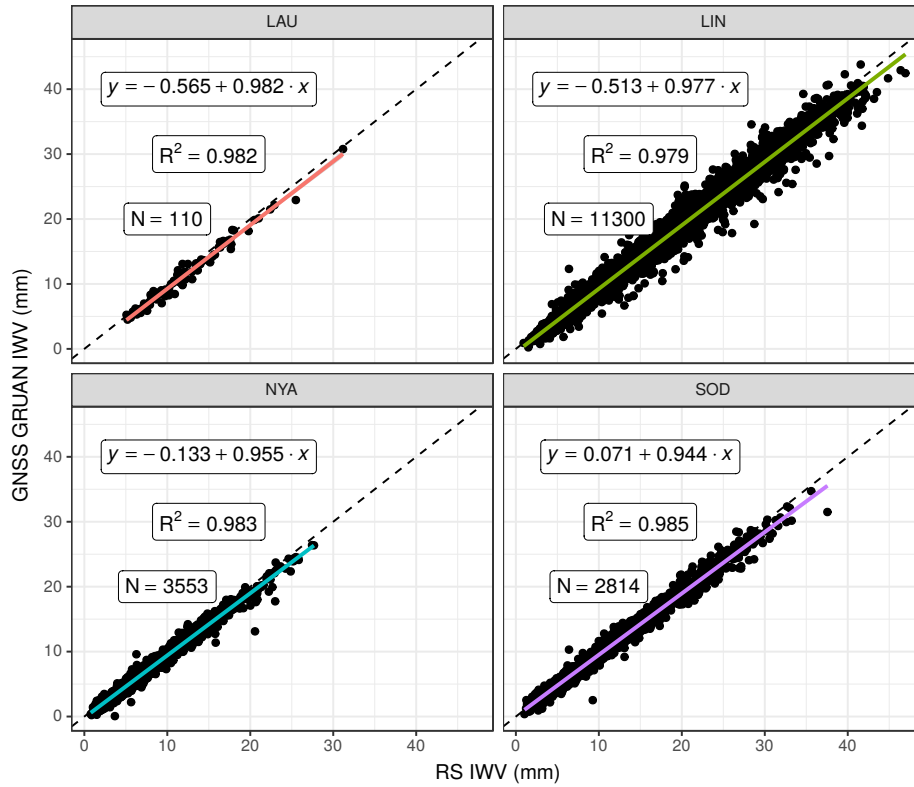


Figure 2: Scatterplots for GNSS IWV data (y-axis) and RS IWV data (x-axis) for the four GRUAN stations. Color, dashed lines are regression lines and black, continuous lines are the identity line.

174        Needless to say, this is only for comparison purposes, since the radiosonde  
 175 meteorological data is typically available for at most four times a day, and the  
 176 GNSS products are available every 15 minutes.

177    3.2. Comparison between GNSS IWV and RS IWV.

178    3.2.1. Overall Statistics and regressions.

179        Table 3 shows a summary of the statistics of the differences between IWV  
 180 from GNSS and RS. MBE values are over  $-0.9$  mm for all stations, being  
 181 closer to zero for NYA and SOD (around  $0.5$  mm). SD values are around  
 182  $0.6 - 1$  mm. Median and MBE values are similar, which indicates that the

Table 3: Statistics of the differences GNSS IWV - RS IWV (all in mm, except slope and R2, which are unitless). MABE is mean absolute bias error, MEDIAN is the median of the differences, IQR is the inter-quartile range of the difference and N the number of data-points.

Site	MBE	SD	MABE	MEDIAN	IQR	N
LAU	-0.767	0.672	0.855	-0.753	0.658	109
LIN	-0.874	1.099	1.094	-0.833	1.150	7837
NYA	-0.492	0.614	0.600	-0.449	0.712	2164
SOD	-0.516	0.830	0.726	-0.435	0.957	2118

183 differences distributions are most likely normal. Figure 2 shows the regression  
 184 lines. Both data-sets are in agreement with  $R^2$  around 0.98.

185 The differences GNSS-RS and relative differences are analyzed in this section  
 186 in order to find dependence on different variables. The differences are distributed  
 187 into bins of similar values of the variable analyzed, and the evolution of MBE  
 188 and SD over the different bins is analyzed. It must be noticed that the data bins  
 189 with less than 15 data are not shown, as they are not considered representative.

### 190 3.2.2. Dependence of GNSS-RS differences on IWV

191 The available data-set have been divided into bins of 5 mm. All stations have  
 192 a very similar behavior with respect to IWV. The relative MBE in Figure 3 (top)  
 193 shows that there is a dry bias (around 5%) that decreases in absolute value with  
 194 IWV. However, for SOD first bin is closer to zero ( $\sim 2.5\%$ ) than the rest of the  
 195 bins ( $\sim 5\%$ ) of SOD. Absolute MBE (not shown) typically increases in absolute  
 196 value with IWV, ranging from less than  $-1$  mm up to  $-2$  or  $-2.5$  mm. Such  
 197 small range explains the behaviour of relative MBE: absolute differences do not  
 198 change much, but the reference IWV does, thus the relative value decrease (in  
 199 absolute value) as IWV increases.

200 Regarding precision (see Figure 3, bottom), relative SD, decrease as IWV  
 201 increases, reaching a minimum of around 5 % in all cases for IWV above 15 mm.

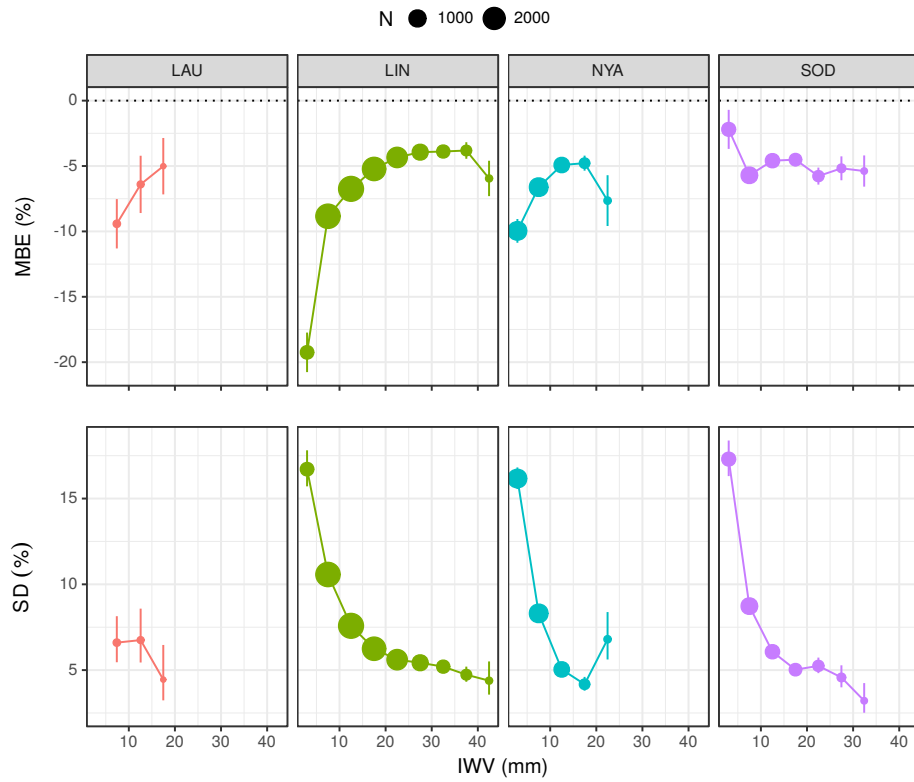


Figure 3: MBE (top) and SD (bottom) of GNSS-RS differences (%) with respect to IWV from RS for the four GRUAN stations.

202 Despite the different ranges of IWV and number of data of each station, the  
203 relative SD is very similar in the lowest bin, between 15 – 17 %). A similar  
204 interpretation to that of the MBE is appropriate here: SD in absolute terms  
205 increases with IWV, but in a range (0.5 – 2 mm) that is quite smaller than the  
206 range of IWV itself (0 – 40 mm), and therefore relative SD tends to decrease  
207 with increasing IWV. Unfortunately, LAU available data does not show a wide  
208 range of IWV, so it is difficult to interpret the results, but they are compatible  
209 with those observed in the rest of sites, with values around 5 – 7 % in the  
210 range of 5 – 20 mm. A similar behaviour was observed in other comparisons  
211 between GNSS and satellite products (Román et al., 2015; Vaquero-Martínez  
212 et al., 2017a,b, 2018) and between RS and satellite products (Antón et al., 2015).  
213 Correlation coefficient  $R$  decreases as IWV increases (not shown), from values  
214 over 0.8 for low IWV to values below 0.7 for IWV above 30 mm.

### 215 *3.2.3. Dependence of GNSS-RS differences on SZA*

216 Differences related to SZA could be due to errors in radiosonde sensors (es-  
217 pecially humidity sensor, which is affected by solar radiation), as stated in Wang  
218 & Zhang (2008) and Dirksen et al. (2014). Figure 4 (top) shows relative MBE  
219 of every 5° bins. It must be noticed that LAU does not have bins with enough  
220 (more than 15) data, so its results are not considered.

221 Although there are some differences between stations, relative MBE gen-  
222 erally worsens as SZA increases. LIN shows a sharp increase at  $SZA = 90^\circ$   
223 (sunrise and sunset), while worsening of MBE with SZA is more monotonous  
224 at SOD and NYA, with some increase from  $110^\circ$ . These behaviours are quite  
225 related to typical values of IWV for those SZA bins, especially at LIN: low SZA  
226 causes higher temperatures, which causes the atmosphere to accept more water  
227 vapor and therefore causes IWV to increase. The distribution of IWV with  
228 SZA was checked, confirming this hypothesis. Also, an interesting feature at  
229 LIN IWV was found: SZA increases rapidly around  $90^\circ$  and decreases for SZA  
230 above that value. As NYA and SOD are Arctic stations, the influence of SZA  
231 is not so marked. Values are typically between 5 and 10 %. GOME-2 water

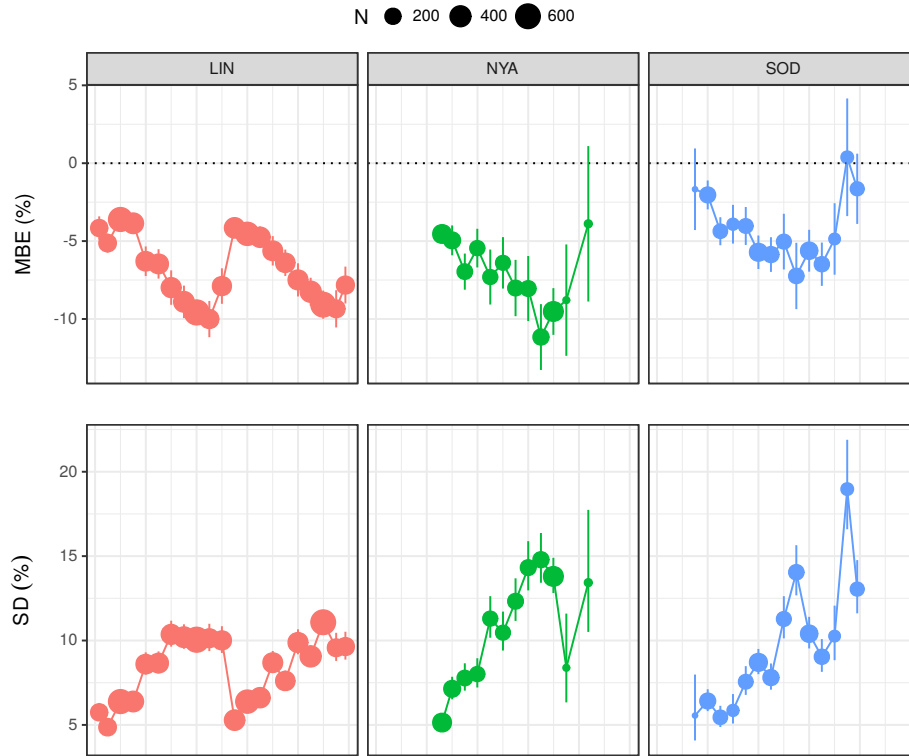


Figure 4: MBE (top) and SD (bottom) of GNSS-RS differences (%) with respect to SZA for three GRUAN stations.

232 vapor product exhibits a similar behavior, as shown in Antón et al. (2015), but  
 233 the sign of MBE is positive in that case. Differences between day and night are  
 234 not important, although in Wang & Zhang (2008) Vaisala RS92 showed a worse  
 235 performance at day than at night.

236 In relative terms, as Figure 4 (bottom) reveals, SD increases with SZA. At  
 237 nighttime, relative SD is higher and more stable, and at daytime, it is lower and  
 238 has a increasing tendency with SZA. Minimum relative SD for all stations is  
 239 around 5%, but the maximum differs (10% for LIN, 15% for NYA, and 20% for  
 240 SOD). This behaviour can be partially due to the observed increase in relative  
 241 SD for low IWV, with a similar argument to the one provided for relative MBE  
 242 in this section. In absolute terms (not shown), SD decreases with SZA, which is

243 consistent with this argument, but it could also be related to the fact that at low  
244 SZA the radiosondes humidity sensor can be affected by solar radiation (Dirksen  
245 et al., 2014; Wang & Zhang, 2008) and partly because of the typically higher  
246 IWV values at low SZA. Several satellite product showed similar behaviour (but  
247 with less precision) (Vaquero-Martínez et al., 2018).

248 In this subsection, it is also analyzed the seasonal dependence of GNSS-RS  
249 differences. SZA and IWV both have annual cycles, which cause the MBE and  
250 SD of the differences between IWV from GNSS and RS to have a seasonal de-  
251 pendence as well. LIN and NYA exhibit (not shown) slightly worse relative  
252 MBE in winter (low IWV) than in summer, while SOD (not shown) has worse  
253 relative MBE at summer (higher IWV). Relative SD in LIN, NYA and SOD  
254 are smaller at summer (low SZA) than in winter. The hypothesis that seasonal  
255 dependence on water vapor products performance is mainly affected by depen-  
256 dences on IWV and SZA is also proposed in other works where satellite products  
257 are compared with GNSS ground-based measurements (Vaquero-Martínez et al.,  
258 2017a,b, 2018).

#### 259 *3.2.4. Dependence on pressure*

260 Surface pressure also affects to the GNSS-RS differences. Figure 5 (top)  
261 shows the MBE each 5 hPa bins. Relative MBE increases without sign as  
262 pressure increases. Values are between  $-15\%$  and  $0\%$  approximately. At  
263 high pressures, MBE worsens at a sharper rate. This could be caused by the  
264 distribution of IWV with surface pressure: at high pressure, IWV is smaller,  
265 being the relative MBE higher. Another explanation that could contribute  
266 partially to this behaviour is related to the way that GNSS IWV is retrieved,  
267 since the surface pressure is needed in Saastamoinen’s model (Saastamoinen,  
268 1972).

269 Relative SD, shown in Figure 5) (top), increases with pressure. Values are  
270 between  $5 - 10\%$  (LIN), around  $10\%$  (NYA) and  $5 - 20\%$  (SOD). LAU shows  
271 slight lower values, around  $5\%$  but these values are only for low IWV pressure  
272 values. As it also happens with MBE, this behaviour could be partially due to

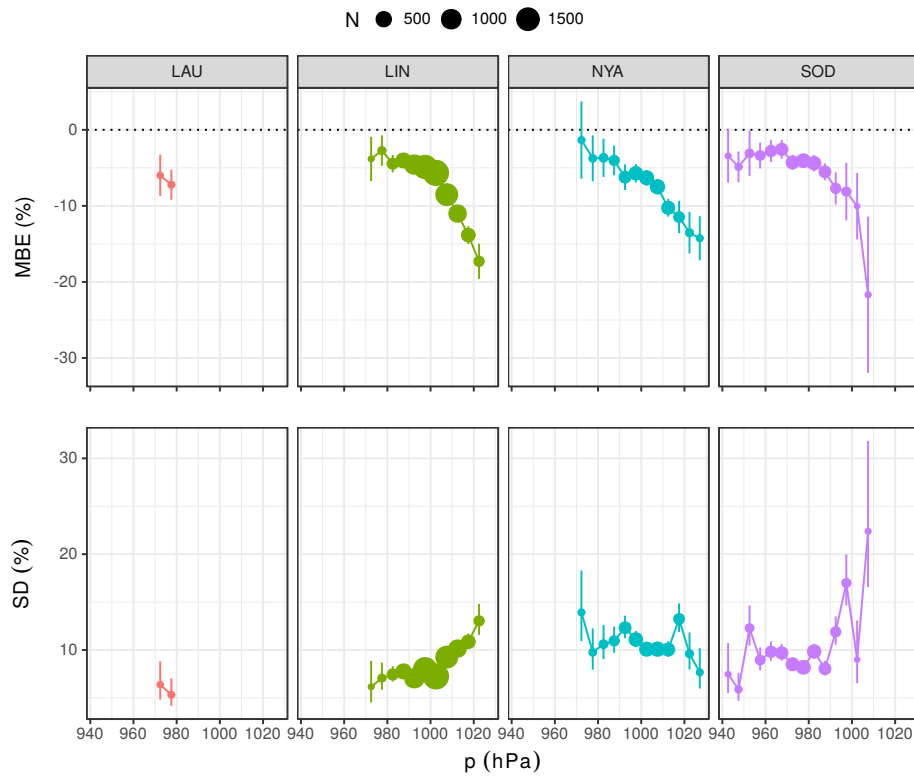


Figure 5: MBE (top) and SD (bottom) of GNSS-RS differences (%) with respect to pressure for the four GRUAN stations.



273 the distribution of IWV with pressure: lower values of IWV are generally reg-  
274 istered at higher values of pressure. SD in absolute terms (not shown) exhibits  
275 a maximum (1000 hPa for LIN ,980 hPa for SOD) that is coincident with a  
276 maximum in typical IWV values.

### 277 *3.2.5. Dependence of GNSS-RS differences on cloudiness*

278 Total cloud cover data have been obtained from Era-Interim Reanalysis (Dee  
279 et al., 2011), and co-located to the sites and times of IWV measurements. These  
280 data are in the form of cloud fraction (CF), that is to say, a number between 0  
281 (no clouds) and 1 (totally covered) indicating the pixel cloud cover.

282 Relative MBE, as shown in Figure 6 (top), is above  $-4\%$  for LIN and SOD,  
283 and between  $-4$  and  $12\%$  for NYA. LAU only counts with 1 point, positive  
284 relative MBE (less than  $2\%$ ). However, the results do not show any dependence  
285 of MBE on CF. MBE in absolute terms does not show any dependence on CF  
286 either.

287 Regarding relative SD, no tendency is observed (see Figure 6 (bottom)).  
288 LIN has very stable values around  $8\%$ . NYA however, have highly variable  
289 values of SD, some around  $7\%$ , other more than  $12\%$ , with high uncertainties.  
290 Nevertheless, SOD exhibits a slight tendency to decrease SD as CF increases,  
291 although still with high variability (between  $7\%$  and  $15\%$ ) and uncertainties.

### 292 *3.2.6. Dependence on radiosonde horizontal movement.*

293 Radiosondes usually move horizontally due to winds. This could be a source  
294 of error (Seidel et al., 2011), so it must be taken into account. The distance  
295 is obtained as the horizontal distance between the first (closest to the ground)  
296 and last (furthest from the ground) radiosonde positions. 20 km bins have been  
297 used to study the evolution of MBE and SD throughout the distances.

298 Figure 7 (top) clearly shows that relative MBE is farther from zero as hor-  
299 izontal displacement increases at NYA, but there is no imporant trend for the  
300 other sites. A reason for this could be that NYA site is located in the Island  
301 of Spitsbergen, meaning that a displacement can put the radiosonde over the

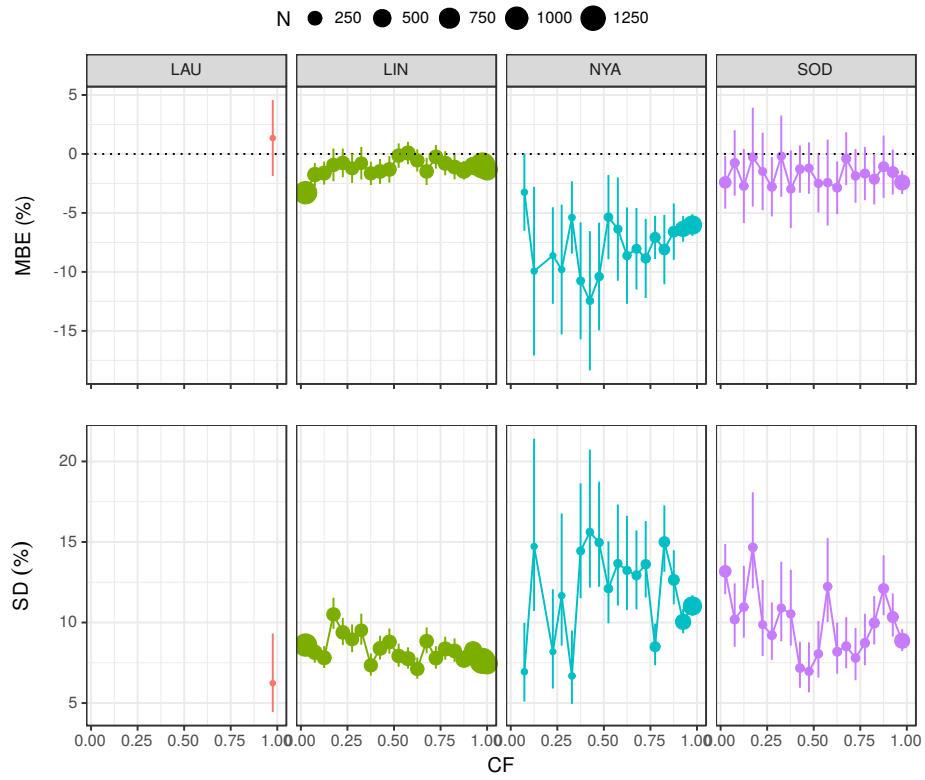


Figure 6: MBE (top) and SD (bottom) of GNSS-RS differences (%) with respect to cloud fraction (CF) for the four GRUAN stations.

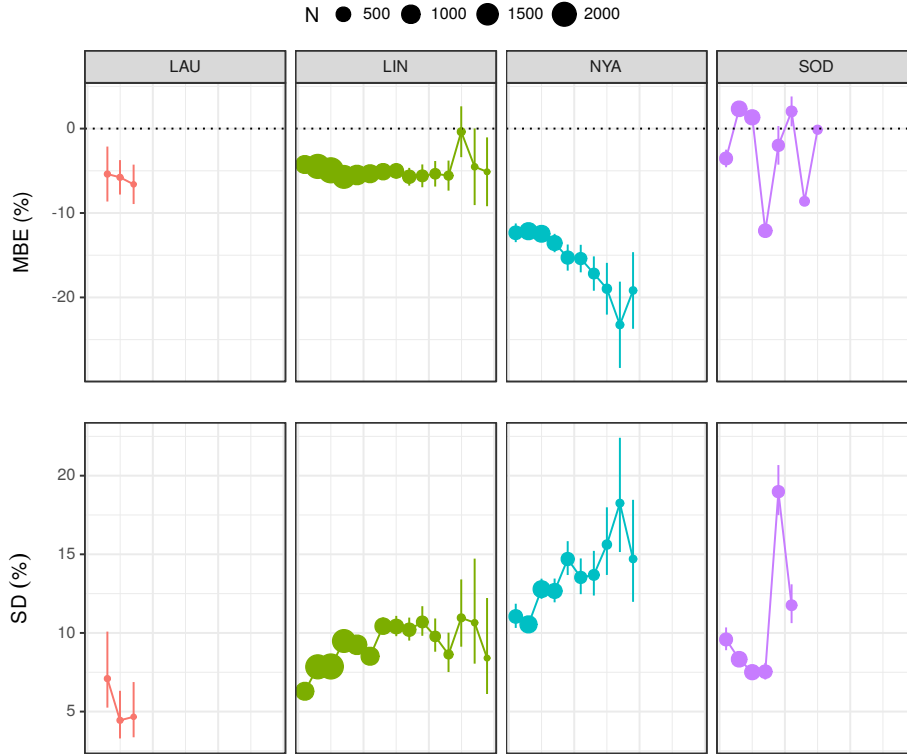


Figure 7: MBE (top) and SD (bottom) of GNSS-RS differences (%) with respect to RS displacement for the four GRUAN stations.

302 sea, where differences with the genuine water vapor vertical profile can be more  
 303 important. SOD shows a very high variability, which could be due to inhomogeneous  
 304 terrain (and thus, humidity) in the vicinity of the site. Relative MBE  
 305 changes from  $-4\%$  to  $-9\%$  at LIN, and from  $-10\%$  to  $-20\%$  at NYA.

306 Figure 7 (bottom) shows the relative SD for several horizontal bins, which  
 307 clearly increases as the horizontal displacement increases, which is to be ex-  
 308 pected. LIN goes from  $5\%$  to  $15\%$ , NYA from  $10\%$  to  $20\%$ , and SOD from  
 309  $0\%$  to  $20\%$ . It must be noted the high variability in SOD relative SD values,  
 310 which can be caused by the inhomogeneity of the humidity fields in the vicinity  
 311 around the site.

312 **4. Conclusions**

313 Global Climate Observing System (GCOS) Reference Upper Air Network  
314 (GRUAN)'s Global Navigation Satellite System (GNSS) and radiosonde (RS)  
315 integrated water vapor (IWV) products are in agreement at the sites considered.  
316 The regression analysis showed a high correlation ( $R^2 > 0.98$ ) and certain offset  
317 that can be due to the spatial separation between GNSS and RS stations. The  
318 intercept is positive for all stations except NYA, and the magnitude ranges  
319 around 0.1 – 0.2 mm. Values of the standard deviation of the differences (SD)  
320 are between 0.6 and 1 mm.

321 The study on dependences of the GNSS-RS differences showed that the mean  
322 of the differences (MBE) and SD generally increase (omitting the sign of MBE)  
323 with IWV, although relative MBE and SD showed the opposed behavior. Per-  
324 formance of RS IWV product was expected to worsen at low solar zenith angle  
325 (SZA) because of errors in humidity sensor of radiosondes but this was not ob-  
326 served, so corrections are being applied correctly. However, SD does increase  
327 at low SZA. Most of the observed dependences on SZA are probably related to  
328 the distribution of IWV with SZA (IWV is larger at low SZA, when the tem-  
329 peratures are higher). The dependences on SZA and IWV also cause a seasonal  
330 dependence.

331 MBE (without sign) and SD exhibits an increase with increasing surface  
332 pressure, that can be partially due to the distribution of IWV with pressure  
333 (IWV is smaller at high pressures), and partially to errors in the modeling of  
334 ZHD through Saastamoinen's model. However, this is an issue that shall be  
335 studied closely in future work. Cloud cover did not show a significant influence  
336 on MBE and SD. Regarding dependence on horizontal displacement of radioson-  
337 des, the relative MBE and SD show that the performance of RS is poorer when  
338 the horizontal displacement is larger, although this seems to be very influence  
339 by the characteristics of the site's vicinity.

340 In summary, the GNSS and RS values are very similar and the dependences  
341 on other factors low, but it should be pointed out that it is still very necessary

342 to have redundant measurements of water vapor in order to improve both the  
343 quality of measurements and the sampling of the data. GNSS exhibits two im-  
344 portant advantages: first the high temporal resolution, and second the stability  
345 against the sky conditions (wind, clouds, etc.), which make GNSS IWV mea-  
346 surement particularly well suited for comparison purposes. However, it must be  
347 noticed that the low number of stations do not allow to extract conclusions over  
348 the whole range of the variables studied, mainly IWV and SZA.

### 349 **Acknowledgments**

350 Support from the Junta de Extremadura (Research Group Grants GR15137)  
351 is gratefully acknowledged. Work at Universidad de Valladolid is supported by  
352 project CMT2015-66742-R. The authors wish to thank the operators at the four  
353 observatories (Lindenberg, Lauder, Ny-Ålesund and Sodankylä) for dutifully  
354 performing reference radiosoundings and maintenance of GNSS according to  
355 the GRUAN standards, as well as GFZ Helmholtz Center Postdam for their  
356 procesing of GNSS data products to obtain ZTD and IWV, and acknowledge  
357 ERA-Interim data.

### 358 **References**

- 359 Antón, M., Loyola, D., Román, R., & Vömel, H. (2015). Validation of GOME-  
360 2/MetOp-A total water vapour column using reference radiosonde data from  
361 the GRUAN network. *Atmospheric Measurement Techniques*, *8*, 1135–1145.  
362 doi:10.5194/amt-8-1135-2015.
- 363 Bevis, M., Businger, S., Herring, T. A., Rocken, C., Anthes, R. A., &  
364 Ware, R. H. (1992). GPS Meteorology: Remote Sensing of Atmospheric  
365 Water Vapor Using the Global Positioning System. *Journal of Geophys-*  
366 *ical Research*, *97*, 15787–15801. URL: [http://doi.wiley.com/10.1029/](http://doi.wiley.com/10.1029/92JD01517)  
367 [92JD01517](http://doi.wiley.com/10.1029/92JD01517). doi:10.1029/92JD01517.

- 368 Boehm, J., Niell, A., Tregoning, P., & Schuh, H. (2006a). Global Mapping  
369 Function (GMF): A new empirical mapping function based on numerical  
370 weather model data. *Geophysical Research Letters*, *33*, 3–6. doi:10.1029/  
371 2005GL025546.
- 372 Boehm, J., Werl, B., & Schuh, H. (2006b). Troposphere mapping functions  
373 for GPS and very long baseline interferometry from European Centre for  
374 Medium-Range Weather Forecasts operational analysis data. *Journal of Geo-*  
375 *physical Research: Solid Earth*, *111*, 1–9. doi:10.1029/2005JB003629.
- 376 Colman, R. (2003). A comparison of climate feedbacks in general cir-  
377 culation models. *Climate Dynamics*, *20*, 865–873. URL: [http://](http://link.springer.com/article/10.1007/s00382-003-0310-z)  
378 [link.springer.com/article/10.1007/s00382-003-0310-z](http://link.springer.com/article/10.1007/s00382-003-0310-z). doi:10.1007/  
379 [s00382-003-0310-z](http://link.springer.com/article/10.1007/s00382-003-0310-z). arXiv:183550600013.
- 380 Colman, R. A. (2015). Climate radiative feedbacks and adjustments at the  
381 Earth’s surface. *Journal of Geophysical Research: Atmospheres*, *120*, 3173–  
382 3182. URL: <http://doi.wiley.com/10.1002/2014JD022896>. doi:10.1002/  
383 2014JD022896.
- 384 Dee, D. P., Uppala, S. M., Simmons, A. J., Berrisford, P., Poli, P., Kobayashi, S.,  
385 Andrae, U., Balmaseda, M. A., Balsamo, G., Bauer, P., Bechtold, P., Beljaars,  
386 A. C. M., van de Berg, L., Bidlot, J., Bormann, N., Delsol, C., Dragani, R.,  
387 Fuentes, M., Geer, A. J., Haimberger, L., Healy, S. B., Hersbach, H., Hólm,  
388 E. V., Isaksen, L., Kallberg, P., Köhler, M., Matricardi, M., McNally,  
389 A. P., Monge-Sanz, B.M., Morcrette, J.-J., Park, B.-K., Peubey, C., de  
390 Rosnay, P., Tavolato, C., Thépaut, J.-N., & Vitart, F. (2011). The ERA-  
391 Interim reanalysis: Configuration and performance of the data assimilation  
392 system. *Quarterly Journal of the Royal Meteorological Society*, *137*, 553–597.  
393 doi:10.1002/qj.828.
- 394 Dirksen, R. J., Sommer, M., Immler, F. J., Hurst, D. F., Kivi, R., & Vömel,  
395 H. (2014). Reference quality upper-air measurements: GRUAN data pro-  
396 cessing for the Vaisala RS92 radiosonde. *Atmospheric Measurement Tech-*

397 *niques*, 7, 4463–4490. URL: <http://www.atmos-meas-tech.net/7/4463/>  
398 2014/. doi:10.5194/amt-7-4463-2014.

399 du Piesanie, A., Pipers, A. J. M., Aben, I., Schrijver, H., Wang, P., & Noël,  
400 S. (2013). Validation of two independent retrievals of SCIAMACHY wa-  
401 ter vapour columns using radiosonde data. *Atmospheric Measurement Tech-*  
402 *niques*, 6, 2925–2940. URL: <http://www.atmos-meas-tech.net/6/2925/>  
403 2013/. doi:10.5194/amt-6-2925-2013.

404 GRUAN (2007). Justification, requirements, siting, and instrumentation  
405 options. URL: [https://www.gruan.org/gruan/editor/documents/gcos/](https://www.gruan.org/gruan/editor/documents/gcos/gcos-112.pdf)  
406 [gcos-112.pdf](https://www.gruan.org/gruan/editor/documents/gcos/gcos-112.pdf).

407 Köpken, C. (2001). Validation of Integrated Water Vapor from Nu-  
408 merical Models Using Ground-Based GPS, SSM/I, and Water Va-  
409 por Radiometer Measurements. *Journal of Applied Meteorology*,  
410 40, 1105–1117. URL: [http://journals.ametsoc.org/doi/abs/10.1175/](http://journals.ametsoc.org/doi/abs/10.1175/1520-0450%282001%29040%3C1105%3AV0IWWF%3E2.0.CO%3B2)  
411 [1520-0450%282001%29040%3C1105%3AV0IWWF%3E2.0.CO%3B2](http://journals.ametsoc.org/doi/abs/10.1175/1520-0450%282001%29040%3C1105%3AV0IWWF%3E2.0.CO%3B2). doi:10.1175/  
412 [1520-0450\(2001\)040<1105:V0IWWF>2.0.CO;2](http://journals.ametsoc.org/doi/abs/10.1175/1520-0450(2001)040<1105:V0IWWF>2.0.CO;2).

413 Myhre, G., Shindell, D., Bréon, F.-M., Collins, W., Fuglestedt, J., Huang, J.,  
414 Koch, D., Lamarque, J.-F., Lee, D., Mendoza, B., Nakajima, T., Robock, A.,  
415 Stephens, G., Takemura, T., & Zhang, H. (2013). Anthropogenic and Natural  
416 Radiative Forcing. In IPCC (Ed.), *Climate Change 2013: The Physical Sci-*  
417 *ence Basis. Contribution of Working Group I to the Fifth Assessment Report*  
418 *of the Intergovernmental Panel on Climate Change* (pp. 659–740). IPCC.  
419 (Ippc ed.).

420 Niell, A. E. (2000). Improved atmospheric mapping functions for  
421 VLBI and GPS. *Earth, Planets and Space*, 52, 699–702. URL:  
422 [http://earth-planets-space.springeropen.com/articles/10.1186/](http://earth-planets-space.springeropen.com/articles/10.1186/BF03352267)  
423 [BF03352267](http://earth-planets-space.springeropen.com/articles/10.1186/BF03352267). doi:10.1186/BF03352267.

424 Ohtani, R., & Naito, I. (2000). Comparisons of GPS-derived precipitable water

425 vapors with radiosonde observations in Japan. *Journal of Geophysical Re-*  
426 *search: Atmospheres*, 105, 26917–26929. URL: [http://doi.wiley.com/10.](http://doi.wiley.com/10.1029/2000JD900362)  
427 1029/2000JD900362. doi:10.1029/2000JD900362.

428 Opaluwa, Y. D., Adejare, Z. A. T., Abazu, I. C., Adewale, T. O., Odesanmi,  
429 A. O., & Okorochoa, V. C. (2013). Comparative Analysis of Five Standard  
430 Dry Tropospheric Delay Models for Estimation of Dry Tropospheric Delay  
431 in Gns Positioning. *American Journal of Geographic Information System*,  
432 (p. 11).

433 Prasad, A. K., & Singh, R. P. (2009). Validation of MODIS Terra,  
434 AIRS, NCEP/DOE AMIP-II Reanalysis-2, and AERONET Sun pho-  
435 tometer derived integrated precipitable water vapor using ground-based  
436 GPS receivers over India. *Journal of Geophysical Research*, 114,  
437 D05107. URL: <http://doi.wiley.com/10.1029/2008JD011230>. doi:10.  
438 1029/2008JD011230. arXiv:16510847.

439 Rama Varma Raja, M. K., Gutman, S. I., Yoe, J. G., McMillin, L. M., & Zhao,  
440 J. (2008). The Validation of AIRS Retrievals of Integrated Precipitable Water  
441 Vapor Using Measurements from a Network of Ground-Based GPS Receivers  
442 over the Contiguous United States. *Journal of Atmospheric and Oceanic*  
443 *Technology*, 25, 416–428. URL: [http://journals.ametsoc.org/doi/abs/](http://journals.ametsoc.org/doi/abs/10.1175/2007JTECHA889.1)  
444 10.1175/2007JTECHA889.1. doi:10.1175/2007JTECHA889.1.

445 Román, R., Antón, M., Cachorro, V., Loyola, D., Ortiz de Galisteo,  
446 J., de Frutos, A., & Romero-Campos, P. (2015). Comparison of to-  
447 tal water vapor column from GOME-2 on MetOp-A against ground-  
448 based GPS measurements at the Iberian Peninsula. *Science of The*  
449 *Total Environment*, 533, 317–328. URL: [http://linkinghub.elsevier.](http://linkinghub.elsevier.com/retrieve/pii/S0048969715303260)  
450 [com/retrieve/pii/S0048969715303260](http://linkinghub.elsevier.com/retrieve/pii/S0048969715303260). doi:10.1016/j.scitotenv.2015.  
451 06.124. arXiv:26172599.

452 Saastamoinen, J. (1972). Atmospheric Correction for the Troposphere and  
453 Stratosphere in Radio Ranging Satellites. In S. W. Henriksen, A. Mancini, &



- 454 B. H. Chovitz (Eds.), *Geophysical Monograph Series* (pp. 247–251). American  
455 Geophysical Union. URL: <http://doi.wiley.com/10.1029/GM015p0247>.  
456 doi:10.1029/GM015p0247.
- 457 Seidel, D. J., Sun, B., Pettey, M., & Reale, A. (2011). Global radiosonde  
458 balloon drift statistics. *Journal of Geophysical Research*, *116*. URL: <http://doi.wiley.com/10.1029/2010JD014891>. doi:10.1029/2010JD014891.
- 460 Vaquero-Martínez, J., Antón, M., Ortiz de Galisteo, J. P., Cachorro, V. E.,  
461 Álvarez-Zapatero, P., Román, R., Loyola, D., Costa, M. J., Wang, H.,  
462 Abad, G. G., & Noël, S. (2018). Inter-comparison of integrated water  
463 vapor from satellite instruments using reference GPS data at the Iberian  
464 Peninsula. *Remote Sensing of Environment*, *204*, 729–740. URL: <http://linkinghub.elsevier.com/retrieve/pii/S0034425717304406>. doi:10.  
465 //linkinghub.elsevier.com/retrieve/pii/S0034425717304406. doi:10.  
466 1016/j.rse.2017.09.028.
- 467 Vaquero-Martínez, J., Antón, M., Ortiz de Galisteo, J. P., Cachorro, V. E.,  
468 Costa, M. J., Román, R., & Bennouna, Y. S. (2017a). Validation of  
469 MODIS integrated water vapor product against reference GPS data at  
470 the Iberian Peninsula. *International Journal of Applied Earth Observation  
471 and Geoinformation*, *63*, 214–221. URL: [http://linkinghub.elsevier.  
472 com/retrieve/pii/S0048969716327176](http://linkinghub.elsevier.com/retrieve/pii/S0048969716327176). doi:10.1016/j.jag.2017.07.008.  
473 arXiv:27988187.
- 474 Vaquero-Martínez, J., Antón, M., Ortiz de Galisteo, J. P., Cachorro, V. E.,  
475 Wang, H., González Abad, G., Román, R., & Costa, M. J. (2017b). Vali-  
476 dation of integrated water vapor from OMI satellite instrument against ref-  
477 erence GPS data at the Iberian Peninsula. *Science of The Total Environ-  
478 ment*, *580*, 857–864. URL: [http://linkinghub.elsevier.com/retrieve/  
479 pii/S0048969716327176](http://linkinghub.elsevier.com/retrieve/pii/S0048969716327176). doi:10.1016/j.scitotenv.2016.12.032.
- 480 Wang, J., & Zhang, L. (2008). Systematic Errors in Global Radiosonde Precip-  
481 itable Water Data from Comparisons with Ground-Based GPS Measurements.

482 *Journal of Climate*, 21, 2218–2238. URL: <http://journals.ametsoc.org/>  
483 [doi/abs/10.1175/2007JCLI1944.1](http://doi.org/10.1175/2007JCLI1944.1). doi:10.1175/2007JCLI1944.1.

484 WMO (2008). Report of the GCOS Reference Upper-Air Network Implemen-  
485 tation Meeting. URL: [https://www.gruan.org/gruan/editor/documents/](https://www.gruan.org/gruan/editor/documents/gcos/gcos-121.pdf)  
486 [gcos/gcos-121.pdf](https://www.gruan.org/gruan/editor/documents/gcos/gcos-121.pdf).